Facile time-of-flight methods for characterizing pulsed superfluid helium droplet beams

Citation	He, Y., Zhang, J., Li, Y., Freund, W. M., & Kong, W. (2015). Facile time-of-flight methods for characterizing pulsed superfluid helium droplet beams. Review of Scientific Instruments, 86(8), 084102. doi:10.1063/1.4928107
DOI	10.1063/1.4928107
Publisher	American Institute of Physics
Version	Version of Record
Terms of Use	http://cdss.library.oregonstate.edu/sa-termsofuse

Facile time-of-flight methods for characterizing pulsed superfluid helium droplet beams

Yunteng He, Jie Zhang, Yang Li, William M. Freund, and Wei Kong[a)]
Department of Chemistry, Oregon State University, Corvallis, Oregon 97331, USA

(Received 19 May 2015; accepted 25 July 2015; published online 11 August 2015)

We present two facile time-of-flight (TOF) methods of detecting superfluid helium droplets and droplets with neutral dopants. Without an electron gun and with only a heated filament and pulsed electrodes, the electron impact ionization TOF mass spectrometer can resolve ionized helium clusters such as He_2^+ and He_4^+, which are signatures of superfluid helium droplets. Without ionizing any helium atoms, multiphoton non-resonant laser ionization of CCl_4 doped in superfluid helium droplets at 266 nm generates complex cluster ions of dopant fragments with helium atoms, including $(He)_nC^+$, $(He)_nCl^+$, and $(He)_nCCl^+$. Using both methods, we have characterized our cryogenic pulsed valve—the Even-Lavie valve. We have observed a primary pulse with larger helium droplets traveling at a slower speed and a rebound pulse with smaller droplets at a faster speed. In addition, the pickup efficiency of dopant is higher for the primary pulse when the nozzle temperature is higher than 13 K, and the total time duration of the doped droplet pulse is only on the order of 20 μs. These results stress the importance of fast and easy characterization of the droplet beam for sensitive measurements such as electron diffraction of doped droplets. © *2015 AIP Publishing LLC.* [http://dx.doi.org/10.1063/1.4928107]

INTRODUCTION

Superfluid helium droplets provide an ultra-cold non-interacting medium for studies of dopants at 0.37 K, and helium nanodroplet isolation spectroscopy has proven a versatile technique for many forms of molecular spectroscopy.[1–3] It has been applied in studies of structures and dynamics of novel systems such as biomolecules, free-radicals, metal clusters, and molecular clusters.[4–8] However, the generation of superfluid helium droplets and confirmation of dopant uptake are still challenging for many new laboratories venturing into this field. For large droplets containing more than millions of helium atoms, Rayleigh scattering can be used to confirm the existence of droplets and to determine the timing of a pulsed beam.[9] However, for effective Rayleigh scattering, an ultraviolet (UV) light source is strongly preferred and efforts in background light reduction are necessary. Fast ion gauges have also been used to confirm the existence of droplets, but the lack of mass information prevents knowledge of the doping status of a droplet beam. A widely used and effective method for detecting both pure and doped droplets is a quadrupole mass spectrometer with a hot filament for electron impact ionization.[10–13] Unfortunately, the cost of a standard quadrupole mass spectrometer is considerable. Several groups have employed a pulsed collimated electron beam coupled with a time-of-flight (TOF) mass spectrometer for studies of pure droplets and doped droplets.[14,15] However, a pulsed collimated electron beam is not easily available, and the need for deflectors to correct the off-axis velocity of the ions further complicates the system. Moreover, to accelerate the electrons for ionization, a transverse field perpendicular to the flight axis is typically used, which could further exacerbate the off-axis velocity of the thus produced ions in the ionization region. Using photoionization, either with a single photon from a synchrotron source or multiple photons in the nanosecond or femtosecond domain, spectroscopic studies of pure droplets and doped droplets have been reported.[16–19] For the purpose of diagnosis, however, many of the light sources are impractical or overly expensive.

Here, we present two facile approaches to detect helium droplets and droplets with neutral dopants using time-of-flight technology. First, we use a heated tungsten filament as an electron source with a pulsed grid for electron impact ionization (EI-TOF). The acceleration field for the ionizing electrons is in-line with the flight axis and in-line with the droplet beam. Consequently, the mass resolution is limited, but helium cluster ions including He_2^+ and He_4^+ can still be separated. This apparatus is easy to operate and economical to build. It requires no deflectors and no collimated electron beam, and it can measure the free drift time of the neutral droplet beam. Second, we use the 4th harmonic of a nanosecond Nd:YAG laser for non-resonant multiphoton ionization (MPI-TOF). The MPI-TOF is miniature in size but has a better mass resolution than the EI-TOF. With several millijoules at 266 nm from a small Nd:YAG laser, the MPI-TOF is blind to pure droplets, but it can resolve complexes formed between fragments of neutral dopants with helium. Using CCl_4 as a sample dopant, we also report some differences between our mass spectra and those from previous reports of laser ionization obtained under much higher laser intensities. The two different TOF mass spectrometers are in different locations along the droplet beam, which enable the comparison of timing and doping conditions. This capability further reveals the existence of a rebound pulse from our droplet source containing smaller clusters with a

a)Author to whom correspondence should be addressed. Electronic mail: wei.kong@oregonstate.edu. Telephone: 541-737-6714.

faster speed. Doping is more effective for larger sized clusters; hence, at higher nozzle temperatures (above 13 K), only the slower primary pulse contains substantial dopant molecules.

EXPERIMENTAL DETAILS

A schematic of our experimental arrangement is shown in Fig. 1. The apparatus combined a superfluid helium droplet source with two homemade Wiley-McLaren type time-of-flight mass spectrometers:[20] one in-line with the droplet beam (EI-TOF) and the other (MPI-TOF) perpendicular to the beam. The droplet source consisted of a pulsed valve (PV) (Digital Technology Trading and Marketing Ltd., E-L-5-8-C-Unmounted Cryogenic Copper Even-Lavie Valve) cryogenically cooled with a closed-cycle helium cryostat (Sumitomo, SRDK-408SW), and the lowest achievable temperature was ~8 K. The driving electric pulse for the valve had a duration of 24.8 μs, controlled by a driver from the same manufacturer (2009 Model Electronic Driver Unit). Superfluid helium droplets were formed by supersonic expansion of helium (Airgas, 99.9995%) through a conical nozzle of 50 μm in diameter with a stagnation pressure of 50 atm. The droplet beam passed through a 2 mm skimmer before entering the pickup chamber. In the pickup chamber, a flexible gas line (6 mm in outside diameter) was routed to the top of a pickup cell of 4 cm in diameter, and two circular apertures of 5 mm in diameter on the wall of the pickup cell were in line with the droplet beam. The vapor of room temperature CCl_4 was controlled by a leak valve, and it was sufficient to just open the leak valve to produce a stable doping pressure. The pickup chamber was separated from the main chamber through a home-made conical cone with a 5 mm opening. The base pressure in the main chamber was below 10^{-6} Torr.

For electron impact ionization, the electron source was a commercial fast ion gauge (Beam Dynamics, Inc., Model FIG-1) rewired for our purpose, although we have also had equal success with a home-made filament and grid. The tungsten filament supplied electrons by running at a constant current of 2.4 A, and the collector grid facing the filament was biased at 51 V to contain the thermal electrons. The droplet beam passed through the space between the filament and the grid. About 12 mm downstream from the electron source were three electrodes A–C separated by 19 mm, and the flight tube was about 43.2 cm long. Electrodes A and C were pulsed from −70 V to 300 V for 4 μs using a DEI PVX-4140 pulse generator, while electrode B was grounded. The negative voltage on electrode A was to prevent electrons from entering the interior of the mass spectrometer. Once the electrons were energized by the positive pulse, ionization was confined to the vicinity of electrode A, and ionized cations were pushed to electrode B. The duration of 4 μs of the ionization pulse was necessary for accumulation of ions around electrode B. As soon as the voltage on electrode C was dropped back to −70 V, all cations accumulated between B and C were attracted to the flight tube, which was biased at a constant voltage of −180 V. Hence, the time-of-flight of the detected ions started at the falling edge of the positive pulse. Ion signals were detected on a chevron-type microchannel plate (MCP) detector.

For laser ionization, we used the fourth harmonic of a Nd:YAG laser (Quantel, Brilliant) at 266 nm and focused the laser beam using a 25 cm cylindrical lens between electrodes E and F. The pulse energy was ~10 mJ and the resulting power density was about 10^{12} W/cm^2. A single power supply was used to bias electrode E at 50 V and electrode F at 24 V. The gap between electrodes E and F was 9 mm to accommodate the whole droplet beam, and the gap between electrode F and the flight tube was only 3 mm. The flight tube was 6 cm long and was grounded. The electrodes and flight tube were attached to a rotatable wheel connected to a Cajon vacuum feedthrough, and they could be moved out of the way of the droplet beam by rotating the rod connected to the wheel. The MCP detector was mounted on a slide movable on a rail system, and it could be retracted to a corner of the chamber using another Cajon feedthrough. The whole assembly fitted inside the bottom half of a cube-shaped chamber, measuring 25 cm in side length.

The apparatus was controlled by an interface card (DAQ NI-PCIe-6320), which sent out a 10 Hz trigger signal to electrodes A and C for the EI-TOF or to the fire and Q-switch control of the laser for the MPI-TOF. A synchronized 5 Hz trigger was sent to the PV and to an input channel of the interface card. A LabView program read the mass spectrum from an oscilloscope (Agilent, DSOX 2004A) and accumulated the droplet signal (PV on) and background signal (PV off) separately based on the input channel of the interface card.

Each mass spectrometer served a different purpose. The EI-TOF was simple to construct and could ionize pure and doped droplets for preliminary diagnosis. However, the mass resolution of this simple setup was limited, and for detailed diagnosis of doped droplets, it was insufficient. The MPI-TOF relied on non-resonant multiphoton ionization, and under the current operating conditions, the laser power density was insufficient to ionize any helium atoms (more than five photons

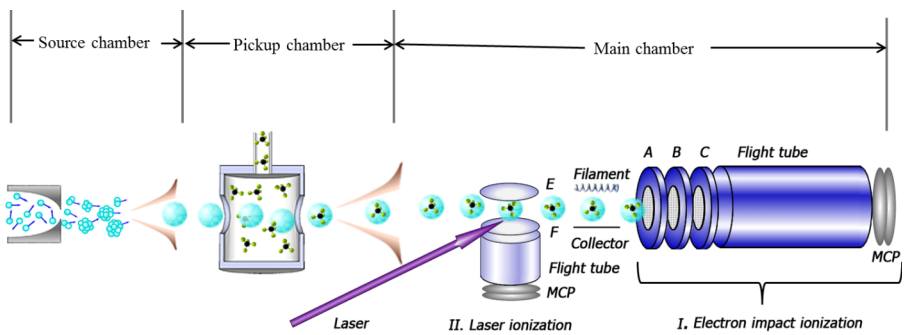

FIG. 1. Schematic diagram of the overall experimental setup including the electron impact ionization and laser ionization time-of-flight mass spectrometers.

are needed), as was confirmed by the lack of any ionization signal with pure droplets. However, with the exception of helium, almost all molecular substances could be ionized with less than three photons at 266 nm. The precise position and timing of a pulsed laser and the easy fulfillment of the spatial focusing condition of the Wiley-McLaren TOF ensured a reasonable mass resolution within the limited space.

RESULTS

Electron impact ionization

In the current configuration of the EI-TOF, the group velocity of the droplet beam was in-line with the flight axis of the EI-TOF; hence, when all electrodes and the flight tube were grounded and the grid was biased at 160 V, we could observe droplet related ions directly arriving at the MCP detector. In fact, at a nozzle temperature of 16 K, we observed two peaks separated by 310 μs on the MCP under this condition, and only when we set the timing of the ionization pulse between the two peaks could we record any mass spectrum containing substantial contributions from He_n^+ with n > 1. Occasionally after changing the kapton gasket or cleaning the nozzle of the pulsed valve, we could observe a single peak when the opening time of the pulsed valve was shortened to less than 23 μs, but the observed beam intensity was typically lower than that when the pulse duration was longer than 24 μs and with the presence of twin peaks. We also noticed the existence of twin peaks when we reconnected the control of the ionizer to the fast ionization gauge. These two peaks could signify velocity slipping between smaller and larger droplets in a bi-modal size distribution,[9,21] or they could represent the primary and a rebound pulse of the pulsed valve.

Fig. 2(a) shows the time-of-flight spectrum of the EI-TOF with (PV on) and without (PV off) pure helium droplets. The temperature of the droplet source was 16 K and the stagnation pressure was 50 atm. Without the droplet beam (PV off), energized electrons can ionize the ambient gas in the main chamber, producing a mass spectrum containing mostly H^+ at 2.105 μs and OH^+ at 8.655 μs from the residual H_2O in the high vacuum chamber. A long tail after the OH^+ is unresolvable, corresponding to masses in the range of 24–100 amu. Although some of these ions can be related to other residue gases such as N_2^+/CO^+, others are possible contaminants from previous experiments in the chamber or on the filament of the fast ionization gauge. When the pulsed valve is on (PV on), both ambient gas and helium droplets can be ionized, and quantitative changes occur in the mass spectrum. The difference between the two traces of PV on and off, as shown in the lower panel of Fig. 2, reveals the fragments related to the droplet, including atomic helium ions and two distinguishable helium cluster ions He_2^+ and He_4^+. These clusters can be considered characteristic signatures of helium droplets.

The mass distribution in Fig. 2 was stable in terms of relative intensities of the different ion fragments when the source temperature of the pulsed valve varied from 8 K to 22 K, although the timing of the ionization pulse had to be adjusted due to the different speeds and hence arrival times of the droplet beam. Above 22 K, the magnitude of the cluster ions dropped precipitously, while the mass peak corresponding to He^+ remained more or less constant for all nozzle temperatures, up to room temperature.

Fig. 3 shows the time profile for the different helium related ions at a source temperature of 16 K. The atomic cation signal contains two peaks, with the first peak more intense and longer lasting. This peak was stable under almost all source temperatures, and it was substantially longer than that of the electrical driving pulse of the valve. The second narrow peak only existed when the nozzle temperature was between 8 and 22 K, and its full-width-at-half-maximum (FWHM) was only ~20 μs. This latter peak also coincided with the main peaks for the clusters He_2^+ and He_4^+. We therefore conclude that only the latter peak contains substantial droplets, while the broader earlier peak contains mainly gaseous helium and a small amount of small droplets.

The conclusion of Fig. 3 shows the importance of mass resolution in characterizing a helium droplet beam. Without the observation of helium clusters, it would be difficult to discern the presence of droplets since ionization from gaseous

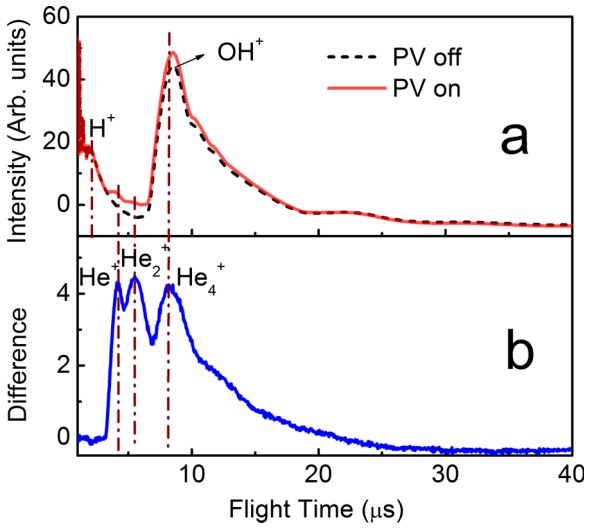

FIG. 2. Electron impact ionization time-of-flight mass spectra of background and pure helium droplets. The top panel shows the mass spectrum of the background (PV off) and that of the droplet beam (PV on) together with the background. The difference in the bottom panel is the net effect of the droplet beam.

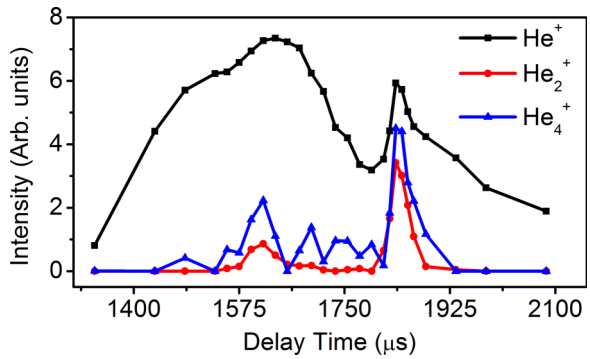

FIG. 3. Time profiles of the different cations He^+, He_2^+, and He_4^+ from the EI-TOF at a source temperature of 16 K. The delay time refers to the time between the electrical trigger signal to the pulsed valve and the time of the electric pulse for ionization.

helium still dominates the total ion signal. Furthermore, the time of arrival of the droplet beam is later than that of gaseous helium, and depending on the flight length between the nozzle and the ionization region, there can be a substantial separation between the gaseous signal and the droplet signal, by up to 600 μs in our case. The duration of the droplet beam is much shorter than that of the gaseous beam, which adds another layer of difficulty for pulsed experiments.

Fig. 4 shows the TOF spectrum when room temperature CCl_4 vapor was introduced into the doping chamber. The pulsed valve was at 16 K with a stagnation pressure of 50 atm. The base pressure of the doping chamber was 10^{-6} Torr, and during doping, the pressure rose to 10^{-5} Torr. Introduction of CCl_4 into the pickup chamber resulted in minimal change in the vacuum level of the main chamber, as confirmed from the comparison of the background spectra with and without doping. The negligible effect of the doping gas in the main chamber was mostly because of the 5 mm cone separating the main chamber from the doping chamber. Moreover, any signal from CCl_4 due to diffusion can be effectively removed when the difference between PV on and PV off is taken, as shown in the lower panel of Fig. 4. Upon doping, both He^+ and He_2^+ are reduced by 25% in the mass spectrum, and the presence of He_4^+ is no longer definitive. Instead, a new fragment of CCl_3^+ due to CCl_4 is observable. The exact time of arrival of the CCl_3^+ fragment, based on the calibration constants of the TOF, is labeled in the figure by the dotted-dashed line; hence, there is no ambiguity about its identity. Its broad width, however, hinders further resolution of other clusters including complexes of CCl_3^+ with helium atoms.

Laser ionization

As explained in the section on "Experimental Details," the intensity of our laser beam was insufficient to ionize helium atoms; hence, the MPI-TOF can only be used to probe doped droplets. The top panel of Fig. 5 shows the MPI-TOF spectra without (PV off) and with (PV on) CCl_4 doped helium droplets, and the lower panel is the net difference between the two spectra. Conditions of the experiment, including the source temperature and stagnation pressure, remained the same as those of Figs. 2–4. Although the flight tube in this MPI-TOF is less than 1/5 the length of that of the EI-TOF, the mass resolution is much higher due to the well-defined small ionization region, the short ionization time (5 ns from the Q-switched Nd:YAG laser), and the spatial focusing conditions of the mass spectrometer. Similar to the EI-TOF spectrum, the background from MPI-TOF also shows a prominent H^+ ion at 1.008 μs due to the presence of perhaps water or H_2 residues in the main chamber. Fragments at flight times of 3.508 μs can be assigned as C^+ and at 5.208 μs as CO^+ or N_2^+. However, a prominent peak at 5 μs is difficult to comprehend, corresponding to a mass of ~25 amu. We suspect that perhaps it is due to contaminants in the chamber from previous experiments, similar to those observed in the long tail of the EI-TOF spectrum in Fig. 2. Upon doping with CCl_4, the mass spectrum remains almost identical, and the difference is only observable after signal subtraction. Part of the reason for the small change is the not-so-ideal level of vacuum in the pickup chamber at 1×10^{-6} Torr. Under this condition, without the "toggle" mode of data collection, it would be impossible to discern the doped signal from the background.

The difference spectrum shows that the most prominent peak is the fragment C^+, followed by Cl^+ and CCl^+. Although CCl_3^+ has the lowest threshold of formation from photoionization of CCl_4, it is not observable in our spectrum, most

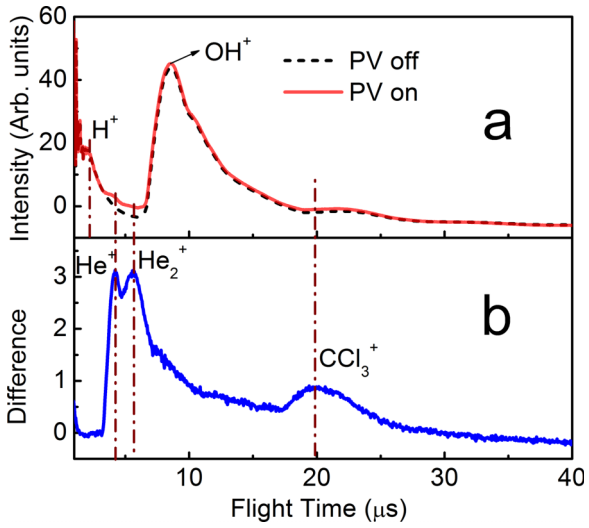

FIG. 4. Electron impact ionization time-of-flight mass spectra of background and doped droplets. The top panel shows the mass spectrum of the background (PV off) and that of CCl_4 doped droplets together with the background. The bottom panel shows the difference—the net effect of the doped droplets.

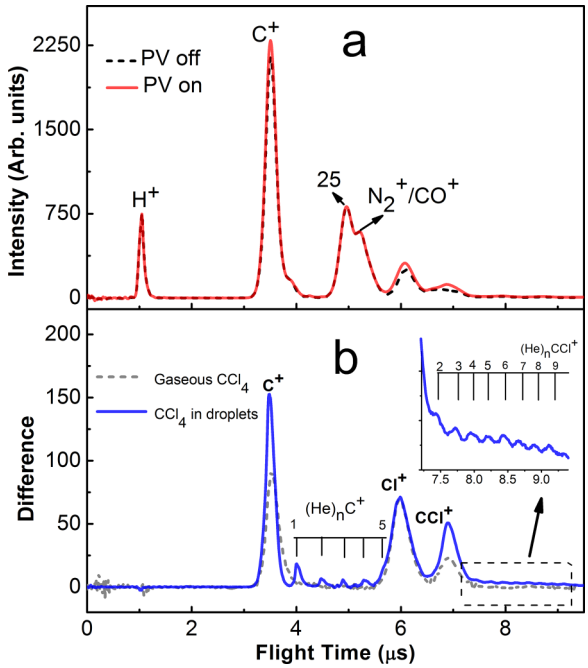

FIG. 5. Multiphoton ionization TOF of helium droplets doped with CCl_4. The top panel shows the mass spectrum of the background (PV off) and that of CCl_4 doped droplets together with the background. The solid line in the bottom panel shows the difference—the net effect of the doped droplets. The dashed grey line shows the mass spectrum of bare CCl_4 recorded by purposely diffusing the gaseous sample into the main chamber, and the signal intensity is normalized for the mass peak of Cl^+.

The difference spectrum shows that the most prominent peak is the fragment C^+, followed by Cl^+ and CCl^+. Although CCl_3^+ has the lowest threshold of formation from photoionization of CCl_4, it is not observable in our spectrum, most

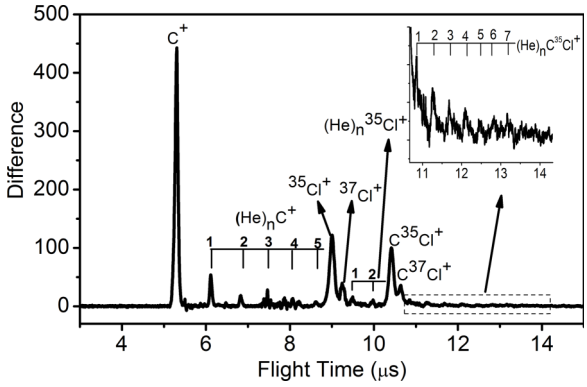

FIG. 6. Multiphoton ionization TOF of helium droplets doped with CCl_4 obtained using a longer flight tube (20 cm instead of 6 cm).

likely because of the abundant photons in the ionization region for subsequent dissociation. More importantly, we observe complexes of C^+ with helium atoms He_nC^+ with n = 1 – 5 and He_nCCl^+ with n = 2 – 9 in Fig. 5(b). In an effort to find the missing complexes of He_nCl^+, we have extended the flight tube to 20 cm by adding an extension tube below the main chamber. Fig. 6 shows the improved mass spectrum, with resolution of the isotopes of chlorine. Complexes of He_nCl^+ can now be identified, albeit small in abundance. The formation of these complexes is only possible from ionization of doped droplets, since the density of CCl_4 in the ionization region should be far below that required for combination with a helium atom.

The dashed grey line in Fig. 5 shows the mass spectrum of bare CCl_4 purposely diffused into the main chamber recorded under the same laser conditions. The spectrum has been scaled for the intensity of the mass peak of Cl^+. The mass spectrum of gaseous CCl_4 contains relatively less C^+ and CCl^+, and in either case, the relative abundance of C^+/Cl^+ is far from 1:4. The relative abundance of Cl^+/CCl^+, however, is close to 3:1 for bare gaseous CCl_4.

We have measured the power dependence of the different fragments as shown in Fig. 7. The relative intensity distribution of the different masses does not show any obvious dependence on the laser power, but the overall signal strength shows a general decrease with decreasing laser power. The experimental data have been fitted with polynomials. With F-test check, C^+ and Cl^+ can be best fitted using second order functions and CHe^+ and CCl^+ can be fitted with third order functions, all with the restriction of forcing the fitting functions through the origin. Energetically, 6 photons are required to strip all chlorine atoms from CCl_4 to form C^+ at 266 nm. The fitting results therefore imply extensive saturation in a few of the intermediate steps. On the other hand, the relative branching ratio of Cl^+ and CCl^+ increases with laser flux, in general agreement with the fact that when more photons are available, CCl^+ can further fragment into Cl^+.

Photoionization of doped helium droplets has been investigated using synchrotron radiations, femtosecond lasers, and nanosecond lasers.[18,19,22] Different approaches seem to follow different ionization mechanisms, with different fragmentation patterns for the same doped species. Our condition with a nanosecond laser at 266 nm in the power density range of 10^{12} W/cm^2 proves to be yet another unique case, with abundant formation of C^+ and without any fragment larger than CCl^+.

Time profile of the Even-Lavie pulsed valve

We have also measured the time profile of the dopant from our droplet beam, using the four most abundant fragments from Fig. 5(b). Figure 8 shows the variation of ion yields as a function of the delay time between the electrical pulse to the pulsed valve and the laser pulse for ionization. The same measurement has also been carried out using the EI-TOF at the same source temperature of 16 K, and very similar time profiles have been obtained, although a time delay of ~300 μs has been observed due to the drift time between the locations of MPI and EI. For all four fragments, Fig. 8 shows a consistent double pulse and a duration of 20 μs for the more intense pulse. This result confirms that the duration of doped droplets is only 20 μs, and that the latter pulse, nearly 200 μs after the earlier pulse, contains more dopant under the current condition.

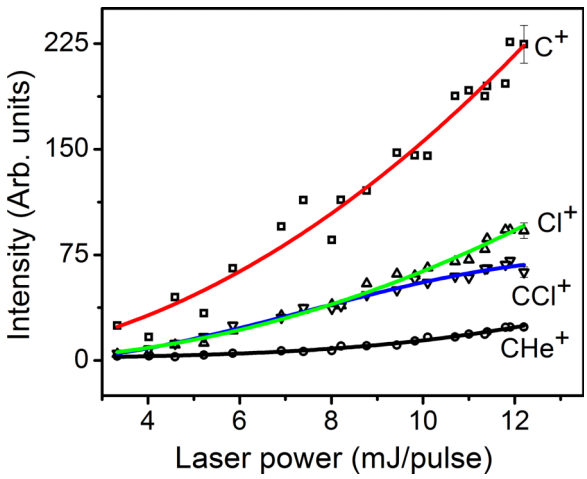

FIG. 7. Power dependent studies of the different fragments from MPI of CCl_4 doped droplets. The solid lines going through the experimental points are fittings using polynomials (C^+ and Cl^+ are second order; CCl^+ and CHe^+ are third order).

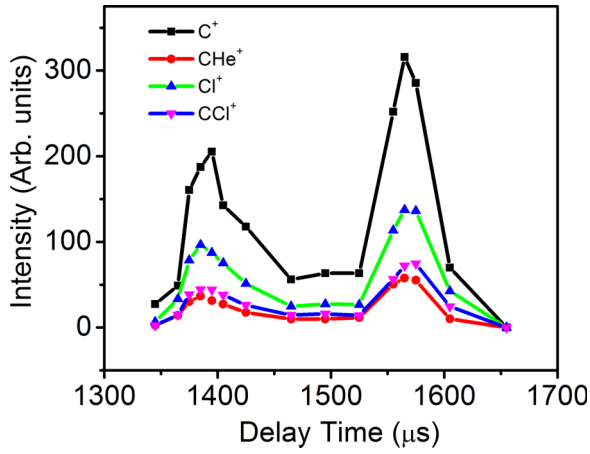

FIG. 8. Time profiles of the different cations C^+, CHe^+, Cl^+, and CCl^+ from the MPI-TOF recorded at a source temperature of 16 K. The delay time refers to the time between the electrical trigger signal to the pulsed valve and the time of the laser pulse for ionization. The latter peak produces more dopant fragments than the earlier one.

We have repeated the same type of measurements at different source temperatures between 8 K and 18 K, and the results are qualitatively the same, always with two droplet pulses. The relative intensities of the two pulses and their separation in timing, however, depended on the source temperature. Below 13 K, the earlier droplet pulse contained more doped ions than the latter droplet pulse, while above 13 K, it was always the latter pulse that contained more droplets. Figure 9 shows a sample profile at 12 K using CBr_4 as dopant. In this case, the earlier pulse contains more dopant than the latter pulse. The time separation of the two droplet pulses progressively gets smaller with increasing source temperature, from 600 μs at 8 K to 100 μs at 18 K.

The twin pulse in the time profile can be analyzed from the available data of the two spectrometers at two different locations along the beam path. As shown in Fig. 1, the MPI-TOF is located in the middle of the main chamber 54 cm from pulse valve, and the EI-TOF is located further downstream, at the exit of the chamber separated by 13 cm from the MPI-TOF. Knowing the timing of the laser pulse and the EI pulse, we can calculate the velocity of the two different droplet pulses: the earlier pulse has a velocity of 452 m/s and the latter pulse of 374 m/s. If we assume that the speeds are the same along the whole travelling distance, we can calculate the exit times of the droplet pulses from the pulsed valve. Knowing the time of the electrical pulse to the pulsed valve, we can then obtain the release time of each droplet pulse. Our numbers indicate that at a source temperature of 16 K, the earlier pulse is released 146 μs after the electrical pulse, and the latter pulse is released 71 μs after the electrical pulse. Thus, the latter pulse is released ~70 μs prior to the earlier pulse at the pulsed valve! Somewhere downstream from the pulsed valve, the two pulses have to overlap and switch in order. To confirm this assessment, we can check the free drift time in the EI-TOF when all electrodes and the flight tube are grounded—an advantage of having the EI-TOF coaxial with the droplet beam. The flight path in the EI-TOF is 46 cm; hence, the droplets drift a total distance of 113 cm to the MCP detector with total flight times of 2635 μs and 2965 μs. Taking the release times of the pulses into consideration, we can then get the velocities of the two groups of ions: 451 m/s and 389 m/s. These numbers agree with the calculated speeds from MPI-TOF/EI-TOF.

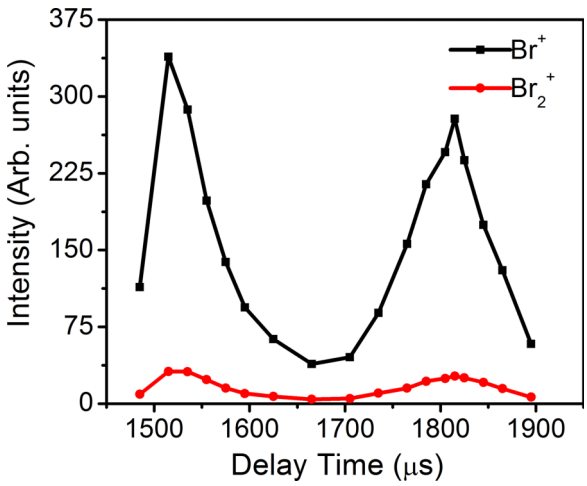

FIG. 9. Time profiles of Br^+ and Br_2^+ from MPI-TOF of CBr_4 doped droplets recorded at a source temperature of 12 K. The delay time refers to the timing between the electrical trigger signal to the pulsed valve and the time of the laser pulse for ionization. Opposite to the case of Fig. 8, the earlier peak generates more dopant fragments than the latter one.

The above situation alludes to an interesting working hypothesis. When the pulsed valve is first opened, larger droplets with a slower speed are initially formed (referred to as the initial or primary pulse in the following), and then the valve has a rebound, and smaller droplets with a faster speed are released (the rebound pulse). The faster rebound group catches up with the slower group, most likely before the skimmer of the source chamber. At a source temperature of 16 K, the location for the overlapping pulses is ~15 cm downstream from the nozzle, just before the skimmer. In the doping chamber, when the source temperature of the pulsed valve is higher than 13 K, the rebound pulse passes through the doping region picking up only a small amount of dopant due to the small sizes of the droplets. The latter primary pulse, on the other hand, has a higher doping efficiency, resulting in abundant dopant in the latter pulse as shown in Fig. 8. Further downstream, in both the MPI and EI experiments, the faster earlier group is actually the rebound pulse, while the slower pulse is the initial pulse with a higher droplet content and larger droplets. At lower source temperatures, on the other hand, even the rebound pulse contains sufficiently large droplets for effective doping. Thus the rebound pulse can result in depletion of dopant molecules in the pickup chamber, thereby decreasing the amount of dopant in the latter primary pulse as shown in Fig. 9.

In a previous report by Pentlehner *et al.*,[9] the Even-Lavie pulsed valve has been fully characterized based on Rayleigh scattering and laser induced fluorescence (LIF). Under most stagnation pressures and source temperatures between 10 and 15 K, double peaks in both Rayleigh scattering and LIF experiments could be observed. Based on the persistence of signal in the latter pulse in the absence of doping or under non-resonant excitation, the authors attributed the latter pulse to Rayleigh scattering of large droplets, and thus established the bimodal size distribution of the droplet source. However, when the source temperature was raised to 20 K and the repetition rate was lowered to 10 Hz, a condition highly unfavorable for Rayleigh scattering, the time profile of the fluorescence still showed a broad shoulder separated by ~40 μs from the main pulse (Fig. 10 of Ref. 9). In general, the double peaks seemed to disappear at high stagnation pressures (above 50 atm) and high repetition rates ($\geq$100 Hz).

At this point, we cannot completely eliminate the possibility of velocity slip and a bimodal size distribution in our droplet beam, and we are unclear if the shoulder peak in the report of Pentlehner *et al.*[9] is the same as the twin peak that we observe in this work. However, there are several pieces of evidence that favor our conclusion of a rebound pulse. First, we observe dopant fragments in both droplet pulses, and the relative intensities of the fragments switch with changing source temperature. We therefore can deduce that there should be a temperature, perhaps around 13 K, that corresponds to equal sized droplets in the two pulses. This is in direct contradiction of bimodal size distribution. Second, the speeds obtained from the free drifting condition, 451 and 389 ± 30 m/s for the two

droplet pulses, and from the timing of ionization between EI and MPI, 452 and 374 m/s, are consistent with the idea of two pulses instead of bifurcation of one pulse. We have also found that by shortening the duration of the electrical control to the pulsed valve, the double pulse can sometimes be combined into one, but the intensity of the droplet beam suffers. This fact further disagrees with the possibility of velocity slip and bimodal size distribution.

A point of concern with cryogenic pulsed valves is the seal between the nozzle component and the valve body. The assembly of both the Even-Lavie valve and the general valve from Parker Hannifin Corp (series 99) requires finger tightening of the nozzle component, which results in inconsistent behavior of the resulting device, even for operation under room temperatures. As illustrated by Pentlehner *et al.*,[9] the time profile of the droplet beam also varies with stagnation pressure and source temperature. It is therefore likely that the difference between the work of Pentlehner *et al.*[9] and our own is due to the different tightness of the nozzle component. It is also possible to suppress the rebound by adjusting the electrical control, the stagnation pressure, and the temperature of the nozzle, but some compromise would have to be made in the droplet size or flux. Improvements in the consistency of the valve assembly are certainly important in eliminating discrepancies regarding pulsed droplet sources.

DISCUSSION

Our EI-TOF is simple to construct and is good enough for rudimentary diagnosis of helium droplet beams. A key component is a pulser that provides a negative offset and a positive pulse to energize thermal electrons for ionization. The frequency of the pulser should be on the order of a MHz, since the time scale of the TOF is on the order of microseconds. The electron source is a tungsten filament supplied with a large current, and the electron collector grid can be of any shape between a coil and a straight piece of wire. The acceleration field for the electrons is in-line with the flight tube; hence, no transverse velocity is gained for the charged particles from the ionization process. Compared with a fast ionization gauge, a commonly used diagnostic tool for molecular beams, the overall cost of our EI-TOF might be higher because of the pulser and the MCP detector, but the additional mass information is valuable, particularly because of the short duration and the complicated time profile of the droplet beam.

In comparison, typical TOF mass spectrometers use collimated electron beams for electron impact ionization. Although a commercial electron gun or beam[23,24] has its advantages in spatial and timing control, it is expensive and largely overkill for diagnostic purposes. Moreover, the acceleration field of the electron beam also introduces a velocity perpendicular to the flight axis for the cations, and to compensate, a set of deflectors is needed downstream from the ionization region. Using an electron beam source coupled with a TOF mass spectrometer, Ellis's group has demonstrated velocity slip in a droplet beam and reported the effect of the nozzle shape on droplet sizes.[21,23] The authors have even suggested size selection based on the time delay between the electrical driving pulse and the firing time of the ionization or excitation beam. Although the mass resolution of our EI-TOF is far inferior to that of commercial mass spectrometers, it is sufficient for identifying signatures of superfluid helium droplets and dopants and for mapping out the time profile of a droplet beam with a time resolution of a microsecond.

The major item in our MPI-TOF is a pulsed Nd:YAG laser. The additional mass resolution afforded by the compact MPI-TOF is appealing for diagnosis of doping conditions. With a moderate laser and by focusing the UV light into the ionization region, almost all molecular species can be ionized, with the exception of helium atoms. Lack of pure helium ions makes the method only sensitive to doped droplets, a unique feature of this setup. The spectrometer can be made miniature in size and can be removed from the interaction region after diagnosis without venting the chamber. These features make it appealing for a quick check prior to any planned experiments.

The key to the success of these two spectrometers is the "toggle" function offered by the interface card. The mass spectrum taken by the oscilloscope is sorted and accumulated in the computer after each ionization event, and instantaneous subtraction effectively removes the background obtained without the droplet beam. Limited by the data transfer protocol of the oscilloscope, however, our highest effective repetition rate is 8 Hz.

CONCLUSION

We have presented two facile methods of detecting superfluid helium droplets and droplets with neutral dopants, both using time-of-flight technology for mass resolution. Without an electron beam and with pulsed electrodes, we have demonstrated electron impact ionization of pure and CCl_4 doped helium droplets with a moderate mass resolution. The information was sufficient to diagnose the droplet beam, with clear indications of helium cluster ions and fragments of dopants. By focusing the 4th harmonic of a pulsed Nd:YAG laser, we have ionized CCl_4 doped in helium droplets and resolved helium complexes with C^+ and other fragments from non-resonant multiphoton ionization. These two spectrometers have been used to measure the time profile of the droplet beam, revealing the existence of an initial primary pulse and a rebound pulse, each with a duration as short as 20 μs. The rebound pulse could overtake the initial pulse prior to doping. When the source temperature was below 13 K, there were sufficient droplets in the rebound pulse to deplete the dopant prior to the arrival of the initial pulse, so the earlier pulse in the MPI and EI profiles contained more dopant. At higher source temperatures, on the other hand, the rebound pulse did not have enough large sized droplets for dopant depletion, and the initial pulse that arrived later than the rebound pulse contained more dopant. Without the mass resolution and the timing information afforded by the mass spectrometers, it would be difficult to capture the detailed behavior of the droplet beam and to precisely determine the timing of dopant containing droplets.

ACKNOWLEDGMENTS

This work is supported by the National Institute of General Medical Sciences (Nos. 1RC1GM092054-01 and

1R01GM101392-01A1) from the National Institutes of Health. The content is solely the responsibility of the authors and does not necessarily represent the official views of the National Institutes of Health. Additional support from the Oregon Nanoscience and Microtechnologies Institute and the Environmental Health Science Center at Oregon State University funded by the National Institute of Environmental Health Sciences (No. ES000210) is also deeply appreciated. We also thank Collin Harthcock in helping with the laser ionization setup. Special thanks are to Dr. Slenczka for his consultation with the performance of the Even-Lavie pulsed valve.

[1]J. P. Toennies and A. F. Vilesov, Annu. Rev. Phys. Chem. **49**, 1 (1998).
[2]J. P. Toennies and A. F. Vilesov, Angew. Chem., Int. Ed. **43**, 2622 (2004).
[3]S. Yang and A. M. Ellis, Chem. Soc. Rev. **42**, 472 (2013).
[4]A. Bartelt, J. D. Close, F. Federmann, N. Quaas, and J. P. Toennies, Phys. Rev. Lett. **77**, 3525 (1996).
[5]J. Tiggesbaeumker and F. Stienkemeier, Phys. Chem. Chem. Phys. **9**, 4748 (2007).
[6]W. Kong, L. Pei, and J. Zhang, Int. Rev. Phys. Chem. **28**, 33 (2009).
[7]F. Bierau, P. Kupser, G. Meijer, and G. von Helden, Phys. Rev. Lett. **105**, 133402 (2010).
[8]M. Goulart, P. Bartl, A. Mauracher, F. Zappa, A. M. Ellis, and P. Scheier, Phys. Chem. Chem. Phys. **15**, 3577 (2013).
[9]D. Pentlehner, R. Riechers, B. Dick, A. Slenczka, U. Even, N. Lavie, R. Brown, and K. Luria, Rev. Sci. Instrum. **80**, 043302 (2009).
[10]H. Buchenau, J. P. Toennies, and J. A. Northby, J. Chem. Phys. **95**, 8134 (1991).
[11]B. E. Callicoatt, K. Forde, T. Ruchti, L. Jung, K. C. Janda, and N. Halberstadt, J. Chem. Phys. **108**, 9371 (1998).
[12]T. Ruchti, K. Forde, B. E. Callicoatt, H. Ludwigs, and K. C. Janda, J. Chem. Phys. **109**, 10679 (1998).
[13]M. N. Slipchenko, S. Kuma, T. Momose, and A. F. Vilesov, Rev. Sci. Instrum. **73**, 3600 (2002).
[14]S. Yang, S. M. Brereton, M. D. Wheeler, and A. M. Ellis, J. Phys. Chem. A **110**, 1791 (2006).
[15]H. Schöbel, P. Bartl, C. Leidlmair, S. Denifl, O. Echt, T. D. Märk, and P. Scheier, Eur. Phys. J. D **63**, 209 (2011).
[16]R. Froechtenicht, U. Henne, J. P. Toennies, A. Ding, M. F. Fieber-Erdmann, and T. Drewello, J. Chem. Phys. **104**, 2548 (1996).
[17]D. S. Peterka, J. H. Kim, C. C. Wang, L. Poisson, and D. M. Neumark, J. Phys. Chem. A **111**, 7449 (2007).
[18]A. Braun and M. Drabbels, J. Chem. Phys. **127**, 114303 (2007).
[19]M. Mudrich and F. Stienkemeier, Int. Rev. Phys. Chem. **33**, 301 (2014).
[20]W. C. Wiley and I. H. McLaren, Rev. Sci. Instrum. **26**, 1150 (1955).
[21]S. Yang and A. M. Ellis, Rev. Sci. Instrum. **79**, 016106 (2008).
[22]D. S. Peterka, J. H. Kim, C. C. Wang, and D. M. Neumark, J. Phys. Chem. B **110**, 19945 (2006).
[23]S. Yang, S. M. Brereton, and A. M. Ellis, Rev. Sci. Instrum. **76**, 104102 (2005).
[24]H. Schöbel, M. Dampc, F. Ferreira da Silva, A. Mauracher, F. Zappa, S. Denifl, T. D. Märk, and P. Scheier, Int. J. Mass Spectrom. **280**, 26 (2009).